IEEE Access
Multidisciplinary ⋮ Rapid Review ⋮ Open Access Journal

Received 12 July 2024, accepted 20 August 2024, date of publication 26 August 2024, date of current version 5 September 2024.

Digital Object Identifier 10.1109/ACCESS.2024.3449996

RESEARCH ARTICLE

Investigating the Effect of Metal Particles and Air Gap Defects on the Surface Charge Distribution of Epoxy Resin Using a Modified Capacitive Probe

FENG WANG[1,2], (Senior Member, IEEE), HUIMIN ZHANG[1], DILIXIATI HAYIREDING[1], HAOCHENG WANG[1], KAIBIN LIANG[2], LIPENG ZHONG[2], (Member, IEEE), HENG YI[2], ZEPING HUANG[2], AND HOUJIE WU[2]

[1]Department of Electronics and Engineering, Yili Normal University, Yining 835000, China
[2]College of Electrical and Information Engineering, Hunan University, Changsha 410082, China

Corresponding author: Kaibin Liang (liangkb@hnu.edu.cn)

This work was supported by the National Natural Science Foundation of China under Grant 52237007.

ABSTRACT Metal particle and air gap defects on the surface of insulators can induce localized electric field distortions and exacerbate charge accumulation, subsequently triggering surface flashover. In this study, we first enhanced traditional capacitive probes to improve stability and effectively suppress charge leakage. The modified probes achieved a charge leakage time constant exceeding 5600 s, with a leakage amount of only 4.9% over a single data acquisition period (210 s). Based on this improvement, we developed a system for measuring surface charges on insulators, investigating the characteristics and influencing factors of surface charge accumulation under metal micro-particles and air gap defects. The results demonstrate that metal micro-particles adhering to the insulator surface accumulate charges of opposite polarity at different locations under applied voltage. These charges tend to diffuse over time and with increased voltage. The presence of air gap defect accelerates charge accumulation in its vicinity, with charge polarity and location being closely related. When the air gap is near the high-voltage electrode, the insulator surface predominantly accumulates positive charges. Conversely, when the air gap is near the ground electrode, negative charges accumulate at both the high-voltage and ground electrodes, with positive charge accumulating in the central region. Both the amplitude and duration of the applied voltage affect the charge accumulation on the air gap surface. Interestingly, with prolonged voltage application, the surface positive charge density in the air gap decreases. Different defect models exhibit charge inversion phenomena occur as the voltage amplitude increases.

INDEX TERMS Surface charge, surface charge measurement, capacitive probe, metal particle, air gap.

I. INTRODUCTION

DC gas-insulated transmission line (GIL) is a crucial method for future large-capacity, long-distance, and cross-regional power transmission. It effectively addresses the challenge of transmitting electric energy between load centers and power centers, thereby promoting the efficient development and utilization of various clean energy sources [1], [2]. Under prolonged DC voltage application, the surface of GIL equipment insulators can accumulate charges, leading to a distortion of the original electric field distribution, which reduces the flashover voltage [3], [4], [5]. Severe accumulation can trigger surface flashovers on the insulator, resulting in serious operational accidents. Metal particles or surface burrs produced during the manufacturing and installation of insulators, as well as air gap defects at the insulator-conductor junctions, can form locally intense electric fields under high external voltages, causing partial discharges. The electrons and positive/negative ions generated by partial discharges are a significant source of surface charge accumulation in

The associate editor coordinating the review of this manuscript and approving it for publication was Bo Pu.

GIL systems [6]. Therefore, the investigation into the effects of localized discharges caused by typical metal particles and air gap defects on charge accumulation at gas-solid interfaces holds substantial theoretical significance for enhancing the understanding of surface charge formation and accumulation mechanisms. Furthermore, these findings provide crucial engineering insights for the design and manufacturing of GIL equipment.

The study of surface charges on insulators must be grounded in the precise measurement of surface potential distribution [7], [8], [9]. The primary methods for measuring the surface potential of insulators include the dust figure method, the Pockels effect method [10], and the electrostatic probe method [11], [12], [13], [14], [15]. The dust figure method cannot quantitatively measure surface charge distribution. The Pockels effect method is limited by the electrostatic relaxation of the Pockels crystal, rendering it suitable only for measuring insulator surface charges under AC or impulse voltages. The electrostatic probe method, a non-contact measurement technique, is widely employed by researchers. Currently, two types of electrostatic probes are commonly used: capacitive electrostatic probes based on the principle of electrostatic induction and Kelvin electrostatic probes utilizing the principle of electrostatic field compensation [16], [17]. While Kelvin probes offer high measurement accuracy, they are expensive and have a limited range. Passive electrostatic probes, with their simple structure and low manufacturing cost, are widely used in applications where high precision in surface charge measurement is not required. However, the key factor affecting the accuracy of capacitive electrostatic probes is the leakage of induced charges to the ground. This leakage can occur along the surface of the supporting insulator, through the insulator body, and via the pins of the operational amplifier, thereby influencing the induced voltage on the central metal rod of the passive probe.

This study developed an electrostatic capacitance probe tailored for detection requirements and integrated it into a measurement system for insulator surface charge, alongside data acquisition and motion control devices. The system enabled measurement and data collection of insulator surface charges. Models were established for surface defects involving metallic particles, air gap defects, and combined defects of metallic particles and air gaps. The study investigated the influence of partial discharge on surface charge accumulation and conducted experimental research using polytetrafluoroethylene (PTFE) insulators. Analysis of experimental data revealed the accumulation patterns of surface charges under different models, facilitating an investigation into how partial discharge affects the characteristics of surface charge accumulation.

II. EXPERIMENTAL METHODS

A. BASIC PRINCIPLE OF ELECTROSTATIC PROBE

Figure 1 presents a schematic diagram of the capacitive probe structure and its equivalent circuit. The primary components include the sensing probe, the shielding cover, and the insulating support between the probe and the shield. In the diagram, C_1 represents the input capacitance for measurement, C_2 denotes the equivalent capacitance between the probe and the insulator surface, and C_3 indicates the equivalent capacitance of the insulator surface charge to the ground. Q represents the charge measured by the probe.

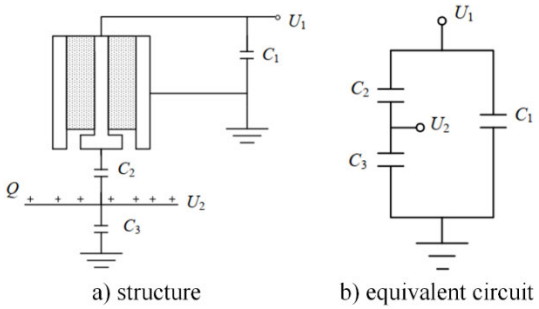

FIGURE 1. Schematic diagram of capacitance probe.

According to Figure 1 (b):

$$U_2 \cdot \left(C_3 + \frac{C_1 C_2}{C_1 + C_2}\right) = Q = \sigma \cdot A \tag{1}$$

In Equation (1), σ represents the surface charge density of the insulator, and A denotes the effective area measured by the probe. According to the principle of capacitive voltage division, we derive:

$$U_1 = \frac{C_2}{C_1 + C_2} U_2 = \frac{C_2}{C_1 C_2 + C_1 C_3 + C_2 C_3} \cdot \sigma \cdot A \tag{2}$$

therefore:

$$\sigma = \frac{C_1 C_2 + C_1 C_3 + C_2 C_3}{C_2 \cdot A} U_1 = M \cdot U_1 \tag{3}$$

$$M = \frac{C_1}{A} \cdot \frac{C_1 C_2 + C_1 C_3 + C_2 C_3}{C_1 C_2} \tag{4}$$

Define M as the scaling factor. If $C_1 \gg C_2$, and $C_2 \gg C_3$, then M can be determined. The value of M can be obtained through calibration experiments.

For the entire surface charge measurement system, Equation (3) reveals that a smaller input capacitance C_1 results in a lower measured charge density by the probe, thereby increasing the charge resolution. Conversely, a smaller probe diameter reduces the effective area A, allowing for measurement in smaller regions. However, this also leads to an increase in measured charge density, which in turn decreases the charge resolution.

B. KEY ISSUES OF THE ELECTROSTATIC PROBE

Figure 1 illustrates the fundamental principle of the classical probe method for measuring surface charge; however, this principle does not account for the influence of resistance within the entire measurement system. Figure 2 presents the equivalent measurement circuit, considering the insulation resistance of the probe R_p, the insulation resistance at the test

circuit's entry point R_b, the input resistance of the operational amplifier R_a, the output resistance of the operational amplifier R_o. Addressing charge leakage is critical in the design of surface charge measurement systems. The primary pathways for charge leakage in the measurement system are: 1) The insulation resistance of the capacitive probe itself; 2) The resistance of the insulating material at the DC operational amplifier pins, which, when a printed circuit board is used to fix the DC operational amplifier, corresponds to the insulation resistance of the printed circuit board; and 3) The input resistance of the DC operational amplifier.

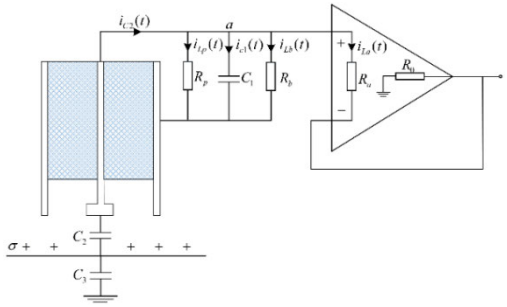

FIGURE 2. Impact of resistance on the measurement circuit.

C. MODIFIED DESIGN OF THE PROBE

The probe designed in this study is illustrated in Figure 3. The main structure comprises a copper probe, an aluminum alloy casing, and polytetrafluoroethylene (PTFE) blocks between them. The probe is used for measurement, the casing needs to be grounded, and the PTFE provides support. Compared to the traditional capacitive probe shown in Figure 1, this design reduces the use of insulating material between the probe and the aluminum alloy shield. This reduction decreases the probe's intrinsic capacitance, thereby enhancing its charge resolution. The elongated front part of the probe facilitates deep insertion into the shielded electrode for insulator measurement, while the thicker rear part helps reduce the input capacitance C, further improving charge resolution. Additionally, small sections of tubular PTFE connect the front and rear of the probe to the aluminum casing, stabilizing the probe within the shield and preventing it from deviating from the center of the front metal tube over time due to gravity. This design minimizes measurement errors and enhances the stability of the measurements.

The capacitive probe structure designed in this study exhibits the following characteristics: 1) The surface leakage distance between the sensing probe and the shield can be increased and adjusted as needed. 2) The majority of the space between the sensing probe and the shield is filled with gas, which reduces the intrinsic capacitance of the probe and enhances the resolution of the charge measurement. Additionally, the reduction in the time constant of charge leakage due to decreased probe capacitance can be compensated by the increased surface leakage resistance. The bias current of operational amplifiers can lead to charge leakage, necessitating the use of operational amplifiers with low bias currents. To mitigate the impact of charge leakage during the measurement process, the probe designed in this study employs the ADA4530-1 operational amplifier, which has a bias current of less than ±20 fA.

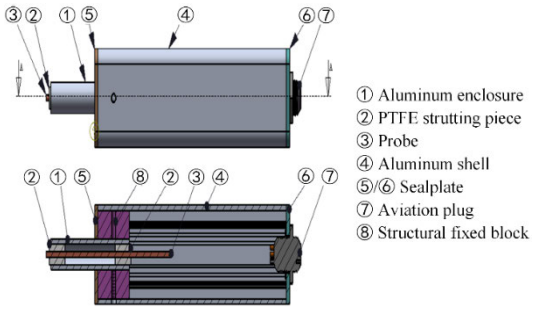

FIGURE 3. The modified probe structure.

D. CHARGE DECAY CHARACTERISTICS

The capacitance value of the input capacitor C1 of the improved electrostatic probe was measured to be 113 pF using high-precision instrumentation. Figure 4 illustrates the temporal variation of charge leakage for the designed probe. At 200 seconds, the probe's measured value decayed from −3.65 V to −3.47 V, corresponding to a charge leakage of approximately 4.9%. After 1200 seconds, the measurement decayed from −3.65 V to −2.90 V, with a charge leakage of about 20.5%, indicating a probe leakage time constant exceeding 5600 seconds (In some cases, a baseline or offset voltage might need to be considered. This is especially relevant if the voltage does not decay all the way to zero but instead levels off at some non-zero value, so $U(t) = U_1 + U_0 e^{-t/\tau}$). The data acquisition time for the experiments designed in this study is approximately 210 seconds, during which the charge leakage is around 4.9%, an acceptable error margin, thus ensuring the probe meets the experimental requirements.

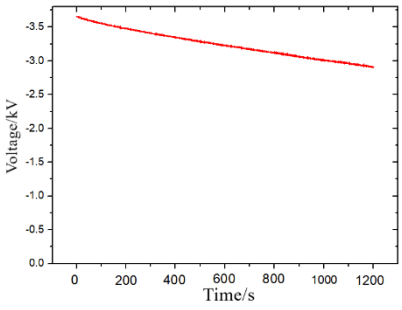

FIGURE 4. Charge leakage characteristics of capacitive probes.

E. CALIBRATION OF CAPACITIVE PROBE

When the electrostatic probe approaches the insulator with accumulated charges on its surface, an induced potential is

generated on the probe. To obtain the surface charge density value of the measured insulator, it is necessary to determine the relationship between the output voltage value of the probe and the charge density of the insulator, namely the scale factor in Equation (4). In this study, we experimentally determined the scaling factor M by substituting the insulator's surface with a metal conductor. The metal conductor was subjected to various DC voltages, and the electrostatic capacitive probe was positioned at a fixed distance of 10 mm from the conductor's surface. A data acquisition card recorded the probe's output voltage at different input voltages. Figure 5 presents the fitted curve depicting the relationship between the voltage U_i on the planar electrode and the output voltage U_O of the probe.

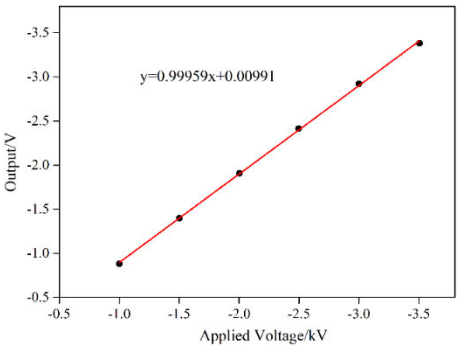

FIGURE 5. The relationship between the input and output of the electrostatic capacitance probe.

It can be obtained that the equation measured in the calibration experiment is $U_O = 0.99959U_i + 0.0991$. The relationship between the output voltage U_O (V) of the probe and the applied voltage U_i (kV) is:

$$\frac{U_1}{U_2} = \frac{C_2}{C_1 + C_2} = 0.00099959 \tag{5}$$

Through the aforementioned experimental measurements, we obtained $C_1 = 113$ pF, which allowed us to calculate $C_2 = 113.1$ fF. Using the parallel plate capacitor formula, the equivalent measurement area of the probe was determined to be 127.91 mm^2, with a radius of 6.38 mm and a measurement distance of 10 mm from the surface. From Equation (4), the calibration factor is derived as follows:

$$M \approx \frac{C_1}{A} = \frac{113 \times 10^{-12}}{127.91 \times 10^{-6}} = 0.883\mu C/(\mathrm{m}^2 \cdot \mathrm{V}) \tag{6}$$

Therefore, the relationship between the output voltage U_O (V) of the probe and the surface charge density σ (μC/m^2) is:

$$\sigma = 0.883 \times (U_1 - 0.0991)\,\mu C/\mathrm{m}^2 \tag{7}$$

F. EXPERIMENTAL PLATFORM AND DEFECT MODEL

The surface charge measurement system, as depicted in Figure 6, employs a motion control apparatus equipped with four stepper motors. These motors enable the rotational movement of the probe, horizontal translation along the forward-backward axis, vertical translation along the up-down axis, and rotational movement of the sample.

Based on the characteristics of insulation defects in GIL, previous researchers have employed four types of simulated insulation defect models, as illustrated in Figure 7(a)-(d). In this study, we focus primarily on investigating defects caused by metal particles on the insulator surface and the presence of air gap defects between the electrode and the insulator. In this study, cylindrical insulators were fabricated using polytetrafluoroethylene (PTFE) material. The dimensions of the insulators were 100 mm in height and 50 mm in diameter.

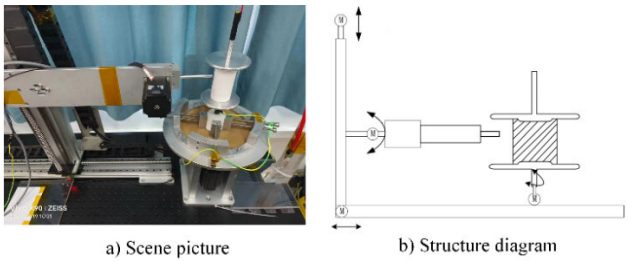

FIGURE 6. The surface charge measurement system.

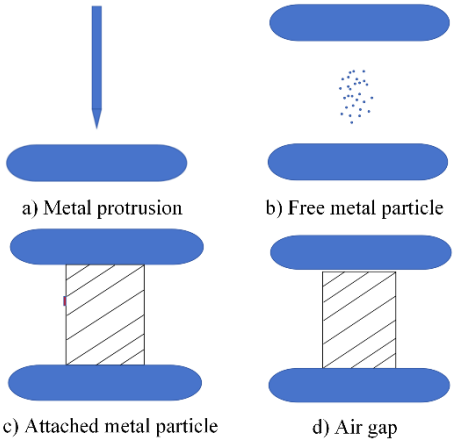

FIGURE 7. Four typical defect models.

III. EXPERIMENTAL RESULTS AND DISCUSSION

A. ACCUMULATION CHARACTERISTICS OF SURFACE CHARGE WITHOUT ARTIFICIAL DEFECTS

As a control group for conditions without artificial defects, negative DC voltages of −10 kV, −20 kV, −30 kV, −40 kV, and −50 kV were applied to the insulator, with each voltage maintained for a duration of 60 minutes. After each measurement, the insulator was cleaned and left to stand at room temperature for over 12 hours to allow complete charge dissipation before conducting the next experiment. The results of these experiments are presented in Figure 8 and surface charge density data are summarized in Table 1.

The experimental results indicate that as the applied voltage increases from −10 kV to −30 kV, the region of negative

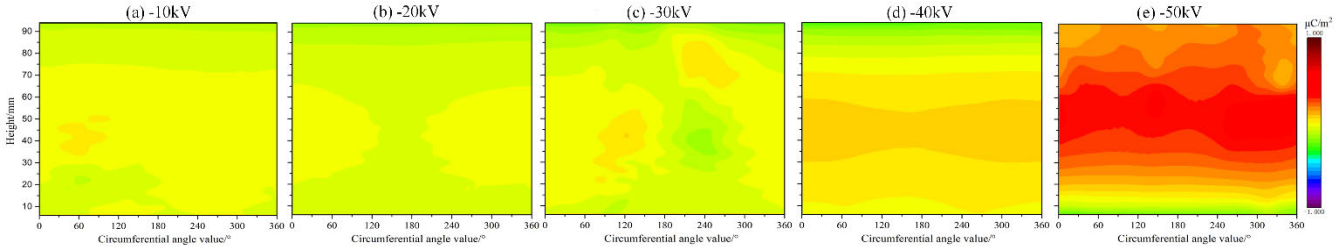

FIGURE 8. The surface charge distribution on insulators under various applied voltages.

charge accumulation primarily expands from the ends near the electrode toward the center. When the voltage is further increased to −50 kV, a polarity reversal occurs, with the predominant surface charge shifting from negative to positive. At −50 kV, the area covered by positive charges on the insulator surface reaches 86.96%. Additionally, both the mean and maximum values of the positive and negative surface charges increase to varying degrees with the rise in voltage.

TABLE 1. Surface charge density data under different voltage.

Voltage	Surface charge density				Area ratio*
	N_{max}	N_{avg}	P_{max}	P_{avg}	
-10kV	-0.1219	-0.0474	0.0362	0.0151	2.32%
-20kV	-0.168	-0.0624	0	0	0%
-30kV	-0.2302	-0.0641	0.0493	0.0184	7.87%
-40kV	-0.2826	-0.0905	0.0618	0.0374	65.79%
-50kV	-0.3044	-0.1501	0.3643	0.1633	86.96%

* Note: Area ratio = (positive charge area/insulator surface area) ×100%

At lower voltage levels, the contribution of gas-side charge conduction to surface charge accumulation is negligible, with surface conduction being the primary pathway for charge accumulation. However, when the voltage reaches −30kV, the gas-side charge conduction significantly enhances surface charge accumulation. At this stage, the positive charges accumulated through gas-side conduction neutralize with the negative charges accumulated via volume conduction. As the voltage level further increases, severe charge accumulation occurs on the insulator surface, likely due to intense local discharges at the triple junction of the electrode-gas-solid insulator. These local discharges generate positive and negative charges that move towards the high-voltage and ground electrodes, respectively, along the surface tangential electric field. Electrons, moving at a higher velocity, can escape the gas-solid interface through electrode conduction, whereas the slower-moving positive charges cannot escape via the conductor, leading to their accumulation. Notably, the positive charge density near the high-voltage electrode is not the highest, possibly due to negative charge generated by partial ionization being captured by positive charges before they can fully accelerate and transfer from the surface to the ground electrode.

To verify the occurrence of partial discharges under different applied voltage amplitudes, we utilized the PPDM3000A portable partial discharge tester provided by Guangdong Youzhi Electric Technology Co., Ltd. The experimental setup is illustrated in Figure 9. Table 2 presents the partial discharge magnitude and frequency for the insulator at various voltage levels. The data indicate that with increasing voltage levels, the maximum apparent charge of partial discharge shows a slight increase, while the discharge frequency per second increases significantly. Specifically, the frequency of discharges rises from 6.5 times per second to 530.6 times per second as the voltage increases, with the maximum discharge quantity (Qmax) escalating from 11.16 pC to 14.04 pC. Notably, starting from −40kV, there is a marked increase in discharge quantity, corresponding to the rapid expansion of the positively charged region on the surface, as depicted in Figure 8(d).

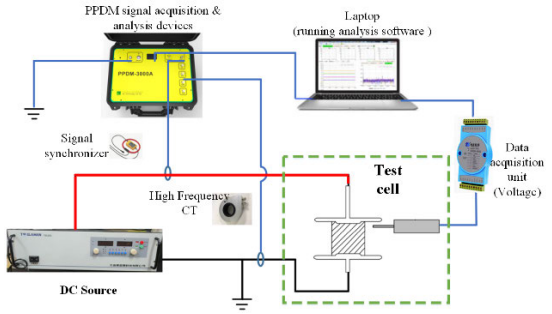

FIGURE 9. The partial discharge measurement platform.

TABLE 2. Partial discharge discharge and discharge frequency.

Voltage (kV)	Qmax(pC)	Npps**
0	11.16	6.5
-10kV	12.99	20.2
-20kV	13.08	33.3
-30kV	12.89	47.4
-40kV	13.66	267.8
-50kV	14.53	421.2

* Note: Npps = Number of discharges per second

Given that partial discharges occurring at excessively high voltages significantly impact surface charge distribution,

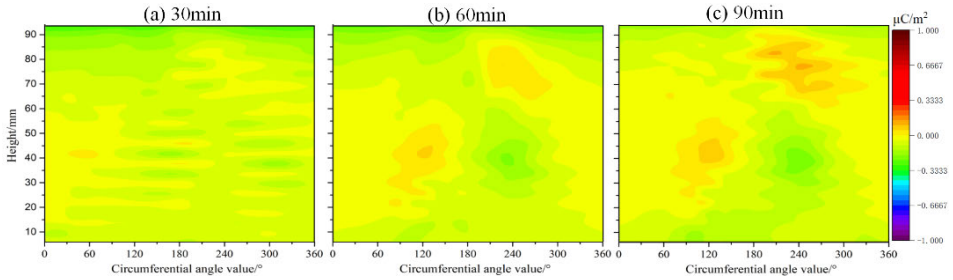

FIGURE 10. The surface charge distribution on insulators under different voltage application durations (−30kV).

subsequent experiments involving gapless insulators in this study will employ an experimental voltage of −30kV.

Figure 10 illustrates the surface charge distribution on polytetrafluoroethylene cylindrical insulators under an applied voltage of −30kV for various exposure durations. The corresponding surface charge density data are presented in Table 3.

The experimental results indicate that the surface charge distribution characteristics of the polytetrafluoroethylene cylindrical insulator model are similar under different durations of applied DC negative voltage. Negative charges accumulate near the high-voltage electrode, while a small amount of positive charges accumulate near the ground electrode. As the application time increases from 30 minutes to 90 minutes, the positive charge density increases and the negative charge density decreases. Specifically, the average negative charge density decreases from −0.0823 μC/m^2 to −0.0643 μC/m^2, while the average positive charge density increases from 0.0080 μC/m^2 to 0.0365 μC/m^2. The maximum negative charge density decreases from −0.3042 μC/m^2 to −0.2210 μC/m^2, and the maximum positive charge density increases from 0.0173 μC/m^2 to 0.1048 μC/m^2. Furthermore, the proportion of the area with positive charges increases from 1.11% to 12.75%. These findings indicate that as the duration of voltage application increases, the accumulation of positive charges on the insulator surface intensifies.

TABLE 3. Surface charge density data under different time duration.

Duration	Surface charge density				Area ratio
	N_{max}	N_{avg}	P_{max}	P_{avg}	
30min	-0.3042	-0.0823	0.0173	0.0080	1.11%
60min	-0.2607	-0.0726	0.0558	0.0208	7.87%
90min	-0.2210	-0.0643	0.1048	0.0365	12.75%

As the duration of the applied voltage increases, both positive and negative charges accumulate on the surface. However, the accumulation of negative charges is generally slower. This discrepancy may be related to the transfer processes of positive and negative charges generated by local discharges at the triple junction. Negative charges consist of electrons and negative ions, with their total charge equaling that of the positive charges. Electrons can partially escape the surface region via conduction through the electrode, whereas positive charges cannot transfer in this manner. Consequently, the region of positive charge accumulation expands over time.

B. ACCUMULATION CHARACTERISTICS OF SURFACE CHARGE IN METAL PARTICLE DEFECT MODEL

To investigate the impact of voltage amplitude on a surface metal particle defect model, linear metal particles were used in the experiment. These particles were copper wires measuring 4 mm in length and 0.5 mm in diameter. To ensure stable adhesion of the metal particles to the insulator surface, they were affixed using 502 adhesive, with the center of the metal wire positioned at a height of 30 mm. Care was taken during the bonding process to prevent the adhesive from spreading and contaminating areas outside the metal wire. The insulator was subjected to negative DC voltages of −10kV, −30kV, and −40kV for a duration of 60 minutes. Figure 11 illustrates the surface charge distribution on the polytetrafluoroethylene cylindrical insulator after 60 minutes under different voltage amplitudes, with the corresponding surface charge density data provided in Table 4.

TABLE 4. Surface charge density data under different voltage.

Voltage (kV)	Surface charge density				Area ratio
	N_{max}	N_{avg}	P_{max}	P_{avg}	
-10	-0.2607	-0.0871	1.1633	0.1819	81.26%
-30	-0.7069	-0.1917	2.1457	0.4150	79.71%
-40	-1.0723	-0.3200	3.1751	0.7566	83.86%

From the experimental results, it is observed that the surface charge distribution of the surface metal particle defect model exhibits similar characteristics under different voltage amplitudes. Compared to configurations without linear metal particles, near the high-voltage electrode, there is still accumulation of like-polarity negative charges. However, influenced by the presence of linear metal particles, near the high-voltage electrode, there is also accumulation of positive charges of opposite polarity to the high-voltage electrode, while areas near the ground electrode accumulate

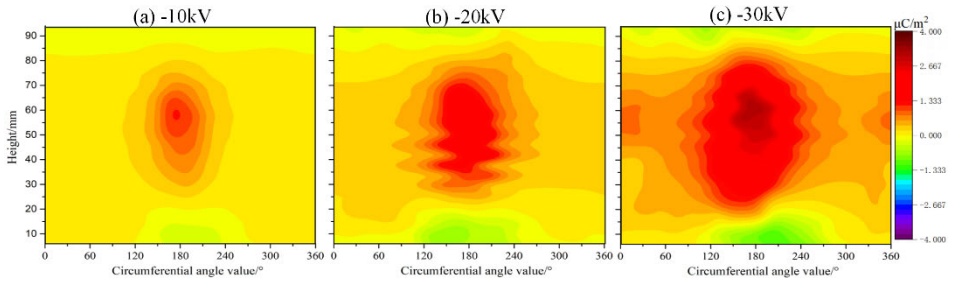

FIGURE 11. The surface charge distribution on insulators under different voltage (with metal particle defect).

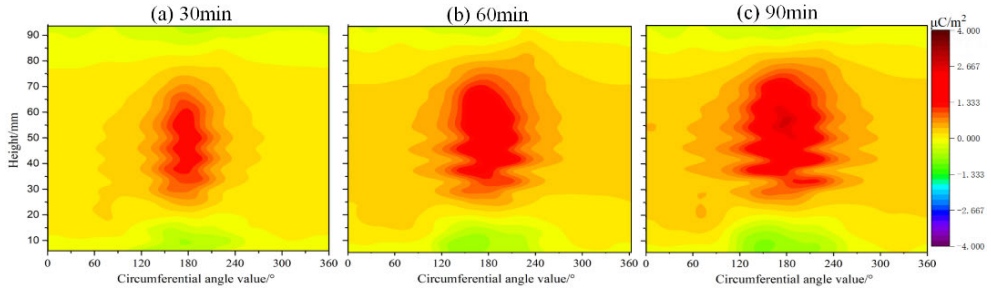

FIGURE 12. The surface charge distribution on insulators with different time duration (with metal particle defect).

like-polarity negative charges. Other regions of the ground electrode continue to accumulate positive charges. As the voltage increases from −10kV to −40kV, the average negative charge density increases from −0.0871 μC/m^2 to −0.32 μC/m^2, and the average positive charge density increases from 0.1819 μC/m^2 to 0.7566 μC/m^2. The maximum negative charge density increases from −0.2607 μC/m^2 to −1.0723 μC/m^2, while the maximum positive charge density increases from 1.1633 μC/m^2 to 3.1751 μC/m^2. These findings indicate that with increasing voltage amplitude, the accumulation of surface charges on the insulator intensifies.

Near the upper edge of the metal particles, positive charges migrate to and accumulate on the surface of the insulator under the influence of the electric field, while negative charges move away. Conversely, near the lower edge of the metal particles, negative charges migrate to the insulator surface and accumulate under the influence of the electric field. This results in a charge accumulation pattern of positive charges above and negative charges below the metal particles, as observed in the experiment. With an increase in voltage level, the accumulation of charges near the metal particles intensifies. This phenomenon arises because higher voltage levels enhance the electric field strength near the edges of the metal particles, thereby increasing gas discharge in that area. As a result, the accumulation of positive and negative charges near the metal particles intensifies along the surface conduction pathway.

Figure 12 illustrates the surface charge distribution on polytetrafluoroethylene cylindrical insulators with metal particle defects under an applied voltage of −30kV for various durations. The corresponding surface charge density data are presented in Table 5.

Based on the experimental results, it is evident that the surface charge distribution of the metal particle defect model exhibits similar characteristics under different durations of applied DC negative voltage. Moreover, as the duration of voltage application increases, there is a pronounced intensification in the accumulation of surface charges on the insulator.

TABLE 5. Surface charge density data under different time duration.

Duration	Surface charge density				Area ratio
	N_{max}	N_{avg}	P_{max}	P_{avg}	
30min	-0.5891	-0.1695	1.3155	0.2636	70.48%
60min	-0.7069	-0.1917	2.1457	0.4150	79.71%
90min	-0.7996	-0.2418	2.6975	0.4981	78.89%

To investigate the influence of the shape and size of metal particles on surface defects, we employed copper particles with linear, square, and circular geometries in our experiments. The linear particles were copper wires measuring 4 mm in length and 0.5 mm in diameter. The square particles were copper sheets with dimensions of 4 mm in length, 4 mm in width, and 0.5 mm in thickness. The circular particles were copper sheets with a diameter of 4 mm and a thickness of 0.5 mm. Each type of particle was subjected to a negative DC voltage of −30 kV for 60 minutes. Figure 13 illustrates the surface charge distribution on PTFE insulators with different

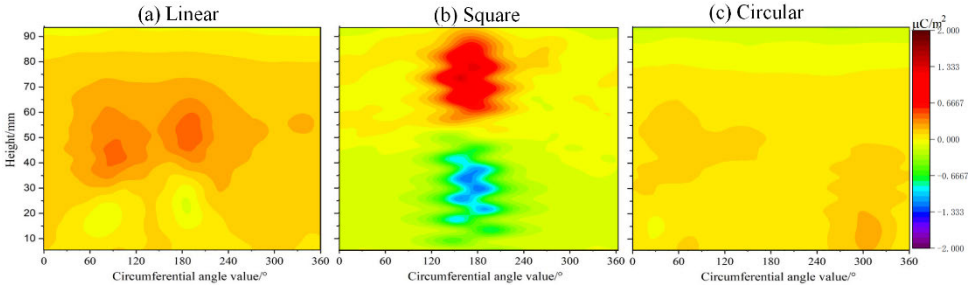

FIGURE 13. The surface charge distribution on insulators with different particle shapes.

shapes of adhered copper particles, the surface charge density data are presented in Table 6.

Experimental results indicate that the surface charge distribution near both linear and square particles exhibits a pronounced accumulation of positive charges above and negative charges below the particles. This accumulation is more intense around the square metallic particles compared to the linear ones. In contrast, the surface charge distribution around circular particles shows no distinct pattern of accumulation except in the vicinity of the high-voltage electrode, where regions of positive charge are observed. This phenomenon can be attributed to the presence of sharp edges on the linear and square particles, which distort the electric field and cause discharge, leading to a similar charge distribution pattern with positive charges above and negative charges below the particles. The smoother edges of the circular particles result in a distribution pattern akin to that observed in the absence of particles, with negative charges localized at the high-voltage electrode and positive charges predominating in other areas.

TABLE 6. Surface charge density data with different particle shapes.

Shape	Surface charge density				Area ratio
	N_{max}	N_{avg}	P_{max}	P_{avg}	
Linear	-0.1152	-0.0349	0.4491	0.1601	92.71%
Square	-1.2271	-0.1893	1.3554	0.2599	24.44%
Circular	-0.2183	-0.0877	0.2600	0.0774	78.79%

To investigate the impact of the position of metal particles on surface charge accumulation, we employed linear copper wires measuring 4 mm in length and 0.5 mm in diameter. The center points of the wires were positioned at heights of 30 mm, 50 mm, and 70 mm, respectively. Each configuration of the insulator was subjected to a negative DC voltage of −30 kV for 60 minutes. The resulting surface charge distributions are depicted in Figure 14, with the corresponding charge density data presented in Table 7.

TABLE 7. Surface charge density data with different particle position.

Distance (mm)	Surface charge density				Area ratio
	N_{max}	N_{avg}	P_{max}	P_{avg}	
30	-0.7069	-0.1917	2.1457	0.4150	79.71%
50	-0.1152	-0.0349	0.4491	0.1601	92.71%
70	-1.5739	-0.2070	1.2993	0.2186	47.92%

Experimental results indicate that while the surface charge accumulation patterns induced by metal particles at different positions share certain similarities, the intensity of accumulation varies. The highest positive charge accumulation of 2.1457 μC/m^2 occurs when the particle is near the ground electrode, while the highest negative charge accumulation of −1.5739 μC/m^2 is observed when the particle is near the high-voltage electrode. When the particle is positioned at the midpoint, both positive and negative charge accumulations are minimal. As previously discussed, gas discharge at the edges of metallic particles in the tangential electric field direction generates significant amounts of positive and negative charges. Positive charges migrate towards the high-voltage electrode, and negative charges migrate towards the

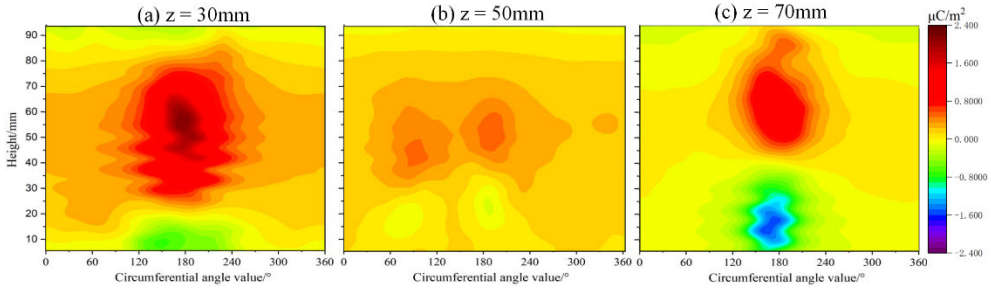

FIGURE 14. The surface charge distribution on insulators with different particle position.

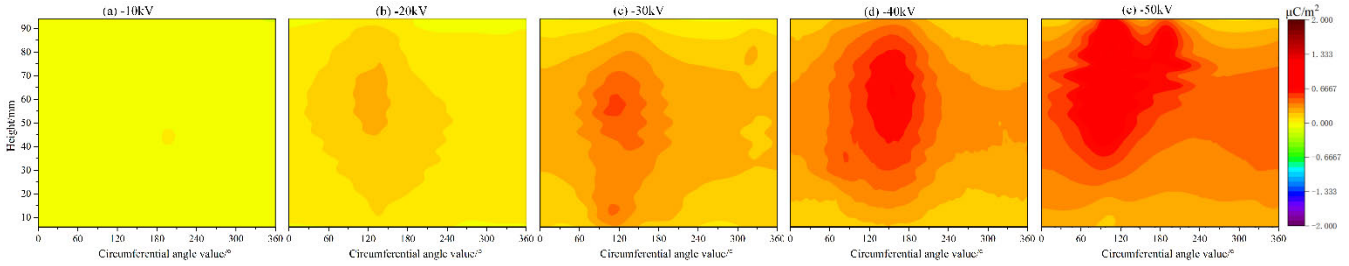

FIGURE 15. The surface charge distribution on insulators with different voltage amplitude.

ground electrode, with partial neutralization occurring near the particle. This results in a distribution pattern of positive charges above and negative charges below. When the particle is near the ground electrode, negative charges migrate directly to the ground electrode, reducing neutralization and leading to more significant positive charge accumulation. Similarly, when the particle is near the high-voltage electrode, negative charge accumulation is more pronounced. At the midpoint position, simultaneous positive and negative charge accumulation and their neutralization result in lower overall charge accumulation.

C. ACCUMULATION CHARACTERISTICS OF SURFACE CHARGE IN AIR GAP DEFECT MODEL

To investigate the influence of voltage amplitude within an air gap defect model, we subjected samples with a 1 mm air gap between the high-voltage electrode and the insulator to various levels of negative DC voltage. The insulators were exposed to voltages of −10 kV, −30 kV, and −50 kV for 60 minutes. Figure 15 illustrates the surface charge distribution on the cylindrical insulators, with the corresponding surface charge data presented in Table 8.

TABLE 8. Surface charge density data under different voltage.

Voltage	Surface charge density				Area ratio
	N_{max}	N_{avg}	P_{max}	P_{avg}	
-10kV	-0.1011	-0.0338	0.0020	0.0015	0.39%
-20kV	-0.0382	-0.0142	0.2157	0.0852	92.85%
-30kV	-0.0177	-0.0120	0.4922	0.2212	97.78%
-40kV	0	0	0.6682	0.3213	100%
-50kV	0	0	1.2024	0.4333	100%

The experimental results indicate that at a voltage amplitude of −10 kV, the area ratio of positive charges is nearly zero, with the surface predominantly covered by negative charges. When the voltage amplitude exceeds −20 kV, the surface charge distribution on the insulator with a 1 mm air gap near the high-voltage electrode shows a trend towards a 100% positive charge area ratio, indicating a predominance of positive charges and their accumulation. As the voltage level increases, both the maximum and average positive charge densities also increase. Conversely, for insulators with an air gap, the maximum and average negative charge densities decrease with increasing voltage, whereas for insulators without an air gap, both the maximum and average negative charge densities increase.

This phenomenon is likely attributable to the onset of partial discharges in the 1 mm air gap near the high-voltage electrode when the voltage exceeds −20 kV. Partial discharge measurements were conducted on insulators with a 1 mm air gap at various voltage levels. The data for these measurements are presented in Table 9.

TABLE 9. Partial discharge discharge and discharge frequency.

Voltage (kV)	Qmax(pC)	Npps
0	10.29	1.3
-10kV	11.45	3.2
-20kV	12.93	66.7
-30kV	13.27	83.9
-40kV	13.52	105.7
-50kV	13.76	119.8

Table 9 suggests that at −10 kV, the voltage level is relatively low, resulting in minimal partial discharge in the air gap near the high-voltage electrode. Consequently, the surface charge distribution resembles that of an insulator without an air gap, predominantly featuring negative charges, with patches of positive charges appearing farther from the high-voltage electrode. However, when the voltage exceeds −20 kV, the partial discharge in the air gap near the high-voltage electrode becomes increasingly severe. This results in a tangential surface electric field directed from the ground electrode towards the high-voltage electrode. The positive and negative charges generated in the air gap then propagate along the surface, ultimately leading to the charge distribution depicted in Figure 15, with positive charge accumulation near the high-voltage electrode.

To investigate the influence of voltage application duration on the air gap defect model, samples with a 1 mm air gap between the high-voltage electrode and the insulator were subjected to negative DC voltages of −50 kV for durations of 30, 60, and 90 minutes. Figure 16 illustrates the surface charge distribution under different voltage

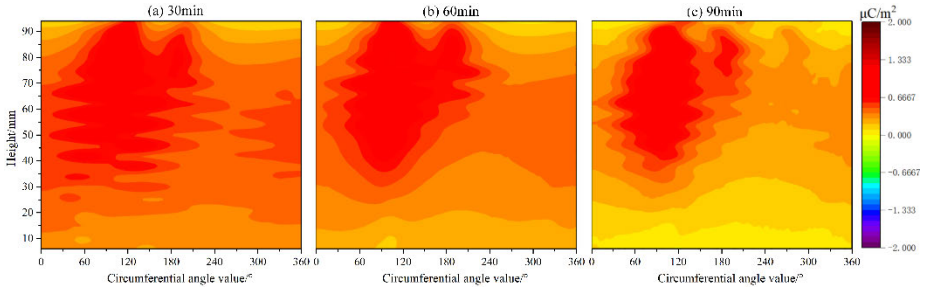

FIGURE 16. The surface charge distribution on insulators with different time duration.

application times. As the duration increases, the maximum positive charge density initially increases slightly and then decreases slightly, showing minimal overall change. Conversely, the average positive charge density begins to decline, and negative charges start to appear on the insulator near the high-voltage electrode air gap.

After 30 minutes of applied voltage, the positive charges begin to saturate, as indicated by the relatively stable maximum positive charge density. Meanwhile, negative charges from the air gap's high-voltage electrode expand directly into the insulator's contact area, leading to a decrease in the average positive charge density and the emergence of negative charge accumulation zones near the high-voltage electrode air gap.

To investigate the effect of air gap size on surface charge accumulation on cylindrical insulators under an applied DC voltage, we conducted experiments using samples with 1 mm and 2 mm air gaps between the high-voltage electrode and the insulator. Both sets of insulators were subjected to a negative DC voltage of −30 kV for 60 minutes. Figure 17 illustrates the resulting surface charge distributions.

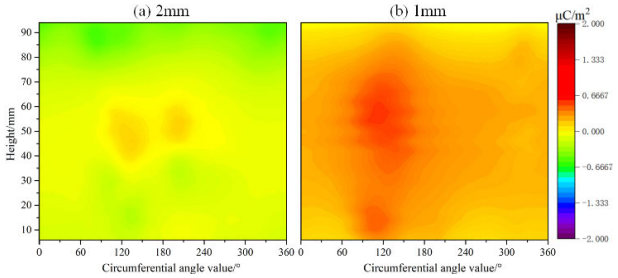

FIGURE 17. The surface charge distribution on insulators with different air gap.

For air gaps of 1 mm and 2 mm, distinct differences in surface charge distribution patterns were observed. In the case of the 1 mm air gap, only a small amount of negative charge accumulated near the high-voltage electrode, with positive charge accumulation dominating the rest of the surface. Conversely, for the 2 mm air gap, negative charge accumulation was observed near both the high-voltage and ground electrodes, with only a small amount of positive charge accumulation in the central region.

While the charge accumulation via bulk conduction was similar for both air gaps, the electric field strength at the air gap was higher for the 1 mm gap compared to the 2 mm gap, resulting in stronger gas ionization. This led to a predominance of positive charges accumulating via the gas-side pathway for the 1 mm air gap, whereas negative charges accumulated via the bulk conduction pathway. Consequently, the surface charge distribution for the 1 mm air gap was primarily positive. In contrast, for the 2 mm air gap, the gas-side accumulated positive charges were less significant than the bulk conduction accumulated negative charges, leading to a predominantly negative surface charge distribution. This accounts for the differing distribution patterns observed for the two air gap sizes.

To investigate the influence of gap positions in the void defect model, experiments were conducted employing two configurations: a 1 mm gap between the high-voltage electrode and the insulator, and a 1 mm gap between the ground electrode and the insulator. Both configurations subjected the insulators to negative polarity DC voltages of −30 kV and −50 kV for 60 minutes. Figure 18 illustrates the surface

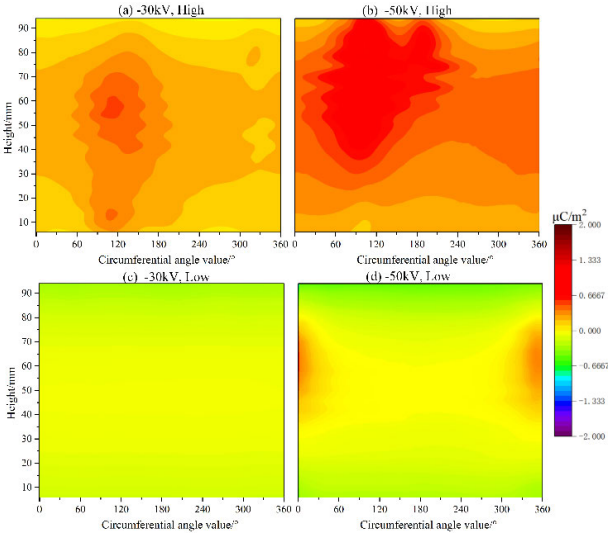

FIGURE 18. The surface charge distribution on insulators with different air gap position.

charge distribution on the insulators, while Table 10 presents statistical data regarding the surface charges.

TABLE 10. Surface charge density data with different air gap position.

Air gap position	Surface charge density				Area ratio
	N_{max}	N_{avg}	P_{max}	P_{avg}	
High, -30kV	-0.0177	-0.0120	0.4922	0.0545	97.78%
High, -50kV	0	0	1.2024	0.4333	100%
Low, -30kV	-0.3106	-0.1129	0	0	0%
Low, -50kV	-0.4751	-0.148	0.3131	0.0951	16.23%

Based on the experimental findings, it is evident that when the gap is present at the high-voltage electrode, the majority of the surface charge consists of positive charges, intensifying with higher voltage levels. Conversely, when the gap is at the ground electrode, the surface charges near both the high-voltage and ground electrodes are negative; however, with increasing voltage levels, positive charge accumulation occurs near the central region close to the high-voltage electrode.

IV. CONCLUSION

This study developed an improved electrostatic capacitance probe, which was used to experimentally investigate the surface charge distribution on insulating materials under negative DC conditions, focusing on two types of defects: metallic micro-particles on the surface and air gaps between the electrode and solid. The main findings are as follows:

(1) In the model with metal particle defects, the charge distribution around the particles is characterized by positive charges at the upper edge and negative charges at the lower edge. This charge accumulation intensifies with increasing voltage levels and duration of voltage application. The shape of the metal particles significantly affects the surface charge distribution. Sharper edges lead to more pronounced accumulation of positive charges at the upper edge and negative charges at the lower edge. The position of the metal particles also influences the charge distribution. Particles near the ground electrode exhibit the highest accumulation of positive charges, while those near the high-voltage electrode show the highest accumulation of negative charges. Particles positioned centrally have the least accumulation of both positive and negative charges.

(1) In the metal particle defect model, there is a distribution characterized by positive charges at the upper edge and negative charges at the lower edge. With increasing voltage levels and exposure time, charge accumulation intensifies. The shape of metallic particles influences surface charge distribution, with sharper edges exacerbating the accumulation of positive charges above and negative charges below. The position of metallic particles also affects surface charge distribution: those near the ground electrode exhibit the greatest accumulation of positive charges above and negative charges below, while those near the high-voltage electrode show the highest accumulation of negative charges above and positive charges below, with particles in central positions showing the least accumulation of both.

(2) In the air gap defect model, near the high-voltage electrode, as voltage levels increase, surface charge distribution transitions from predominantly low-density negative charges to entirely positive charges, with a noticeable accumulation of positive charges near the high-voltage electrode adjacent to the gap. With increased voltage exposure time, surface charge distribution exhibits similarity, although the peak density of positive charges initially increases slightly before decreasing, while the average density of positive charges decreases. Different gap sizes result in varied surface charge distribution patterns: for a 1mm gap, stronger gas-side conduction leads to predominantly positive surface charge distribution, whereas for a 2 mm gap, there is relatively less positive and more negative surface charge distribution. The location of the gap also influences surface charge distribution: gaps at the high-voltage electrode result in predominantly positive surface charges, intensifying with higher voltage levels; gaps at the ground electrode result in surface charges being negative near both the high-voltage and ground electrodes, with positive charge accumulation in the central region increasing with higher voltage levels.

REFERENCES

[1] T. Magier, M. Tenzer, and H. Koch, "Direct current gas-insulated transmission lines," *IEEE Trans. Power Del.*, vol. 33, no. 1, pp. 440–446, Feb. 2018.

[2] H. Koch, F. Goll, T. Magier, and K. Juhre, "Technical aspects of gas insulated transmission lines and application of new insulating gases," *IEEE Trans. Dielectr. Electr. Insul.*, vol. 25, no. 4, pp. 1448–1453, Aug. 2018.

[3] J. Sun, S. Song, J. Zheng, Z. Li, J. Huo, Y. Wang, P. Xiao, S. Akram, and D. Qin, "A review on surface flashover phenomena at DC voltage in vacuum and compressed gas," *IEEE Trans. Dielectr. Electr. Insul.*, vol. 29, no. 1, pp. 1–14, Feb. 2022.

[4] B. Zhang, Y. Li, D. Min, T. Wang, K. Li, G. Zhang, S. Li, X. Li, and A. B. Murphy, "Insight into charge-induced flashover at the gas–solid interface in DC gas-insulated systems," *J. Phys. D, Appl. Phys.*, vol. 57, no. 10, Mar. 2024, Art. no. 103001.

[5] X. Li, C. Cao, and X. Lin, "Influence of conducting particle on DC flashover characteristics and tracking property of GIS/GIL insulator," *IEEE Access*, vol. 10, pp. 17212–17220, 2022.

[6] B. Zhang, Z. Qi, and G. Zhang, "Charge accumulation patterns on spacer surface in HVDC gas-insulated system: Dominant uniform charging and random charge speckles," *IEEE Trans. Dielectr. Electr. Insul.*, vol. 24, no. 2, pp. 1229–1238, Apr. 2017.

[7] P. Molinie, "Measuring and modeling transient insulator response to charging: The contribution of surface potential studies," *IEEE Trans. Dielectr. Electr. Insul.*, vol. 12, no. 5, pp. 939–950, Oct. 2005.

[8] S. Kumara, S. Alam, I. R. Hoque, Y. V. Serdyuk, and S. M. Gubanski, "DC flashover characteristics of a polymeric insulator in presence of surface charges," *IEEE Trans. Dielectr. Electr. Insul.*, vol. 19, no. 3, pp. 1084–1090, Jun. 2012.

[9] B. Zhang and G. Zhang, "Interpretation of the surface charge decay kinetics on insulators with different neutralization mechanisms," *J. Appl. Phys.*, vol. 121, 2017, Art. no. 105105.

[10] Y. Zhu, T. Takada, K. Sakai, and D. Tu, "The dynamic measurement of surface charge distribution deposited from partial discharge in air by pockels effect technique," *J. Phys. D, Appl. Phys.*, vol. 29, no. 11, pp. 2892–2900, Nov. 1996.

[11] A. Kumada, S. Okabe, and K. Hidaka, "Resolution and signal processing technique of surface charge density measurement with electrostatic probe," *IEEE Trans. Dielectr. Electr. Insul.*, vol. 11, no. 1, pp. 122–129, Feb. 2004.

[12] A. Kumada, S. Okabe, and K. Hidaka, "Influences of probe geometry and experimental errors on spatial resolution of surface charge measurement with electrostatic probe," *IEEE Trans. Dielectr. Electr. Insul.*, vol. 12, no. 6, pp. 1172–1181, Dec. 2005.
[13] N. C. Jaitly and T. S. Sudarshan, "In-situ insulator surface charge measurements in dielectric bridged vacuum gaps using an electrostatic probe," *IEEE Trans. Electr. Insul.*, vol. 23, no. 2, pp. 261–273, Apr. 1988.
[14] D. Li, G. Zhang, T. Wang, Y. Hou, and B. Zhang, "Surface charge measurement under AC voltage using active electrostatic probe and controllable phase truncation scheme," *IEEE Trans. Dielectr. Electr. Insul.*, vol. 27, no. 2, pp. 684–691, Apr. 2020.
[15] L. Zhang, D. Yu, D. Tang, and Z. Zhang, "Effect of electrostatic probe online measurement on surface charge distribution for HVDC GIL," *IEEE Trans. Dielectr. Electr. Insul.*, vol. 31, no. 2, pp. 1003–1011, Apr. 2024.
[16] B. Martin and H. Kliem, "Space charge measurements with the scanning Kelvin probe," *IEEE Trans. Dielectr. Electr. Insul.*, vol. 15, no. 2, pp. 560–567, Apr. 2008.
[17] J. Lü, E. Delamarche, L. Eng, R. Bennewitz, E. Meyer, and H.-J. Güntherodt, "Kelvin probe force microscopy on surfaces: Investigation of the surface potential of self-assembled monolayers on gold," *Langmuir*, vol. 15, no. 23, pp. 8184–8188, Nov. 1999.

FENG WANG (Senior Member, IEEE) was born in Liaoning, China, in 1972. He received the B.Sc. and Ph.D. degrees in electrical engineering from Xi'an Jiaotong University, Xi'an, China, in 1994 and 2003, respectively.

He is currently a Professor with the Department of Electronics and Engineering, Yili Normal University, and also with the College of Electrical and Information Engineering, Hunan University, Changsha, China. His research interests include electric arc and intelligent monitoring and diagnosis of power systems.

HUIMIN ZHANG was born in Shandong, China, in 2001. She received the bachelor's degree from Department of Electronic and Engineering, Yili Normal University, in 2023, where she is currently pursuing the master's degree in the field of radio physics.

Her research interests include signal and information processing and its application in power equipment and surface discharge dissipation techniques.

DILIXIATI HAYIREDING received the B.E. degree in wind energy and power engineering and the M.E. degree in renewable energy science engineering from Hehai University, Nanjing, China, in 2014 and 2017, respectively. He is currently pursuing the Ph.D. degree in electronic information engineering with Anhui University, Hefei, China.

Since 2017, he has been with the School of Electronics and Engineering, Yili Normal University, as a Lecturer. His research interests include signal and information processing and its application in power systems.

HAOCHENG WANG was born in Xinjiang, China, in 1992. He received the B.Sc. degree in wind energy and power engineering from Xinjiang University, Urumqi, China, and the M.Sc. degree in electrical engineering, in 2020. He is currently a Lecturer with the Department of Electronics and Engineering, Yili Normal University, China. His current research interests include grid-connected converter control and the stability control of renewable energy power generation systems.

KAIBIN LIANG was born in Hunan, China, in 1990. He received the B.Sc. and M.Sc. degrees in electrical engineering from the School of Electrical Engineering, Wuhan University, Wuhan, China, in 2012 and 2016, respectively, and the Ph.D. degree in electrical engineering, in 2023. He was with PetroChina, in 2013, and State Grid, from 2016 to 2019. He continued his work as a Postdoctoral Researcher with Hunan University, Changsha, China. His research interests include power equipment intelligent monitoring and diagnosis and surface discharge dissipation technique.

LIPENG ZHONG (Member, IEEE) was born in Hunan, China, in 1990. He received the B.Sc. and Ph.D. degrees in electrical engineering from Xi'an Jiaotong University, Xi'an, China, in 2012 and 2017, respectively. He is currently an Associate Professor with Hunan University, Changsha, China. His research interests include air discharge, high-voltage insulation, and online monitoring for power equipment.

HENG YI was born in Hunan, China, in 1997. He received the B.S. and M.S. degrees from North China Electric Power University, China, in 2020 and 2023, respectively. He is currently pursuing the Ph.D. degree with Hunan University, Changsha, China. His research interests online monitoring of power equipment and surface discharge dissipation technique.

ZEPING HUANG was born in Fujian, China, in 1997. He received the B.S. and M.S. degrees from Xiamen University of Technology, China, in 2020 and 2023, respectively. He is currently pursuing the Ph.D. degree with Hunan University, Changsha, China. His research interests include air discharge, high-voltage insulation, and online monitoring of power equipment.

HOUJIE WU was born in Hunan, China, in 1992. He received the M.S. degree from Hunan University, China, in 2024. His research interests online monitoring of power equipment and surface discharge dissipation technique.